

**EFFECTS OF MAGHNITE NANOCCLAY MODIFICATION AND  
COMPATIBILIZATION ON THE PHYSICAL AND MORPHOLOGICAL  
PROPERTIES OF POLY(VINYL CHLORIDE)/POLY(ETHYLENE-CO-VINYL  
ACETATE) BLENDS**

I. Bouaziz<sup>1,2</sup>, R. Doufnoune<sup>\*1,2</sup>, N. Haddaoui<sup>3</sup>, D. Benachour<sup>4</sup>, F. J. Baltá-Calleja<sup>5</sup>

<sup>1</sup>URMES, Equipe de Valorisation des Polymères, Université Ferhat ABBAS Sétif-1, Algérie

<sup>2</sup>Département de Génie des Procédés, Université Ferhat ABBAS Sétif-1, Algérie

<sup>3</sup>Laboratoire LPCHP, Faculté de Technologie, Université Ferhat ABBAS Sétif-1, Algérie

<sup>4</sup>Laboratoire LMPMP, Faculté de Technologie, Université Ferhat ABBAS Sétif-1, Algérie

Instituto de Estructura de la Materia, CSIC, Serrano 119, 28006 Madrid, Spain

Received: 21 October 2018 / Accepted: 21 December 2018 / Published online: 01 January 2019

**ABSTRACT**

In this research work poly(vinyl chloride)(PVC), ethylene vinyl acetate copolymer (EVA), and Maghnite nanoclay (MGT) were used to prepare PVC/EVA nanocomposites. The MGT clay was intercalated with octadecyltrimethylammonium chloride (ODTMA) and grafted with  $\gamma$ -aminopropyltriethoxysilane (APTES). The blend nanocomposites were prepared through the melt mixing of PVC/EVA blend at a weight ratio of 50/50 (wt%/wt%) with 20 wt% of compatibilizer; ethylene vinyl acetate grafted with an alcohol (EVA-g-OH) and 3 wt% of modified MGT clay using a Brabender plastograph. The nanocomposites so prepared were characterized using X-ray diffraction, TGA/DTA, mechanical tests and SEM. The results showed that when PVC was blended with EVA, with the modified MGT and with the compatibilizer, synergistic effects in the thermal stability and mechanical properties were observed.

**Keywords:** Nanocomposites; PVC; EVA; Maghnite nanoclay; Modification; Compatibilizer.

Author Correspondence, e-mail: [doufnoune@yahoo.fr](mailto:doufnoune@yahoo.fr)

doi: <http://dx.doi.org/10.4314/jfas.v11i1.22>



## 1. INTRODUCTION

Polymer/layered silicate-nanocomposites (PLSN) have received extensive academic and industrial attention over the last 20 years. Most electrical, mechanical properties, permeability, flame retardancy and thermal stability that are expected in these nanocomposites depend on the dispersion of the reinforcing fillers within the polymer matrix with the use of just small amounts of clay (typically less than 5 wt%). The intrinsic properties as well as the high specific area of the filler participate in the chemical reactions with the polymer [1-3]. Currently; a special attention is given to polymers filled with smectic clays such as montmorillonite and bentonite as innovative materials for industrial applications.

Montmorillonite (MMT) has been widely investigated because it is environmentally friendly and naturally abundant, and also because of its high exchange capacity and high surface area. Its crystal structure consists of layers made up of two silica tetrahedral sheets fused to an edge-shared octahedral sheet of either alumina or magnesium hydroxide. Stacking of the layers leads to a regular van der Waals gap between them (the interlayer or gallery). Isomorphic substitution within the layers generates charge deficiency, which is compensated by cations absorbed between the three-layer clay mineral sandwiches [4,5].

The compatibility between the polymer and the clay is a crucial factor to obtain well dispersed nanocomposites. Montmorillonite which has a hydrophilic nature, has been found to improve compatibility and reinforces the interaction between the clay and an organic environment and reduce the tendency of clay agglomeration during dispersion [6-8]. The exchange in the clay using surfactants is one alternative to change the hydrophilic characteristic to a hydrophobic one. However, physical, electrostatic interactions and van der Waals forces between the clay layers are reduced within the interlayer space, facilitating, therefore, the polymer chain intercalation which leads to a nanocomposite with an intercalated and or exfoliated nanostructure [3,9].

PVC is a commodity plastic and extraordinarily useful as a commercial material [10,11] because of its properties such as non-flammability, versatility and relatively low cost. However, some drawbacks of PVC such as its poor processability, low impact strength, low thermal stability and brittleness, limit its applications. Furthermore, plasticizers such as

di(2-ethylhexyl) phthalate (DOP) which are added to impart elasticity to PVC, can migrate from the bulk of a packaging material into the packed product and, therefore, can cause health consequences [12]. The problem of migration can make an inappropriate product for many applications [13]. To improve these shortcomings, the incorporation of elastomers in PVC matrix is a very efficient way to avoid using a low molecular weight plasticizer and, therefore, prolong the service life of PVC [6,14]. EVA, which is a thermoplastic elastomer with good mechanical properties, high impact resistance and a very good elasticity, is widely used as plasticizer to convert a rigid polymer into a flexible or semi-flexible material [4,15,16]. Ethylene is non-polar and crystallizable, but vinyl-acetate is polar and non crystallizable. Therefore, their copolymerization will restrict the ability of crystallization of the resulting copolymer [10]. Moreover, the properties of this copolymer (EVA) depend on the content of vinyl acetate (VA) [17].

To develop a new combination of properties and materials with specific enhanced properties, one effective way is blending [10,18]. PVC/EVA blends are an interesting subject of study and deserve special attention due to their complex miscibility and possibility of mixing with a filler to obtain nanocomposites [12,13,16,19-22]. It has been reported that the content of VA influences the compatibility with PVC and increase the interaction between PVC and EVA [14]. It is known that PVC/EVA is a miscible blend when the content of vinyl acetate ranges between 45 and 75% molar [6,13,19]. However, when the blend is obtained by melt mixing it will not be miscible, and compatibilization is required to obtain desired properties [10].

Corradini et al. [22] verified that when the content of VA in EVA is 20% molar and when EVA is completely hydrolyzed, its blend with PVC is therefore almost miscible. Michalski et al. [16] determined the surface free energy of PVC/EVA blend with (70%) of VA. They found that this mixture is miscible in a wide composition range starting with 25% EVA.

Ren et al. [11] used Maleic Anhydride–Styrene–Vinyl Acetate (MAStVA) as a compatibilizer of PVC/EVA blend. They found that PVC/EVA reached miscibility with a concentration of 5-10% by weight of MASTVA.

Ren et al. [23] investigated a melt blending of PVC/VA/organophilic montmorillonite (OMMT) nanocomposites by the masterbatch process. The results indicate that

PVC/VA/OMMT nanocomposites with exfoliated structure have been successfully prepared, whilst partially intercalated and partially exfoliated PVC/OMMT nanocomposites have been produced. The compatibilized nanocomposites show higher values of tensile strength, elongation at break and impact strength than non-compatibilized nanocomposites, and nanocomposites containing more compatibilizer display better mechanical properties. In order to obtain good mechanical properties, the OMMT content should be kept below 5phr.

In some cases the presence of clay in polymers such as polyolefins is not enough to enhance nanocomposites performance. That's why it is necessary to introduce a phase compatibilizer in order to create suitable interactions between the polymer and the polar surface of the clay [1].

Presently, the addition of small amounts of maleic anhydride grafted polyolefins which are miscible with a polymeric matrix, is the most promising strategy since the polar character of the anhydride maleated polyolefin makes it react as compatibilizer and increases the affinity between the filler and the matrix [1,10,24]. The present paper aims to report a new approach for the compatibilization of PVC/EVA blend-clay nanocomposites. Mechanical, thermal and morphological properties of the obtained nanocomposites are also investigated.

## 2. EXPERIMENTAL

### 2.1. Materials and methods

The PVC used is a suspension grade with a K-value of 65-67 and was provided from ENIP Skikda- Algeria. Ba, Ca, Zn and dibasic lead stearate  $2\text{PbO} \cdot \text{Pb}(\text{C}_{17}\text{H}_{35}\text{COO})_2$  were used as thermal stabilizers and lubricants, respectively. The EVA used (grade Hanwha 1316 with VA content 19%) was supplied from Dow company (South Korea). Montmorillonite clay or raw-Maghnite (MGT) with a cationic exchange capacity CEC of 80-90 mequiv/100g was supplied by Roussel in Maghnia (West of Algeria). Octadecyltrimethylammonium bromide (ODTMA, 98% purity),  $\gamma$ -aminopropyltriethoxysilane (APTES, > 99%), dicumyl peroxide (DCP, 98%), maleic anhydride (MAH, 99%), and 1,12- dodecanediol (99%) were purchased from Sigma-Aldrich. All other reagents were laboratory grades and were supplied from Sigma-Aldrich and used without further purification unless otherwise specified. The maleic and alcohol functionalized compatibilizers were prepared in our laboratory as it will be

described in the corresponding section.

## 2.2. Preparation of sodium Maghnite (Na<sup>+</sup>-MGT)

Raw-Maghnite (20 g) was crushed for 20 min using a Prolabo ceramic balls grinder. It was then dried for 2 h at 105°C. The Maghnite was carefully dispersed in a 1M NaCl solution by stirring for about 24 h and separated by centrifugation. This procedure was repeated 4 times to achieve an exchange close to 98-99%. The sediment of the Na<sup>+</sup>-exchanged clay mineral was washed with distilled water and then centrifuged at 3000 rpm for 2 h. The resulting exchanged clay was dispersed into fresh distilled water to become Cl<sup>-</sup> free. Then, the bulk of the water was removed by oven drying at 105°C for 12 h.

## 2.3. Preparation of the organically-modified clay

Natural Na<sup>+</sup>-GMT is hydrophilic and not compatible with most organic molecules. The sodium cation in the interlayer space of montmorillonite can be exchanged with organic cations to yield organophilic montmorillonite. The organoclay was prepared by the following procedure: 10 g of Na<sup>+</sup>-GMT was first dispersed in 1000 ml of deionized water then stirred with a magnetic stirrer at 500 rpm for about 24 h. A pre-dissolved stoichiometric amount of ODTMA solution was slowly added to the clay suspension at 80°C, and then this mixture was vigorously stirred for 3 h. The concentration of ODTMA used was 1 CEC (Cation Exchange Capacity). The product was filtered and washed with hot water, dried at room temperature, ground in an agate mortar and stored in a vacuum desiccator. The ODTMA<sup>+</sup> ion pre-intercalated Maghnite was denoted as ODTMA<sup>+</sup>-MGT.

The modification of ODTMA<sup>+</sup>-MGT with APTES silane coupling agent was carried out by the following procedure: APTES was dissolved in 250 ml in a mixture of water/methanol at a ratio of 75:25. 2 g of ODTMA<sup>+</sup>-MGT was then added to the vessel and the suspension was stirred during 24 h at 80°C. The homogenous mixture was filtrated and then was washed with distilled water and ethanol. Finally the product was dried in a vacuum oven at 100°C for 24 h. The modified ODTMA<sup>+</sup>-MGT prepared from the silane is denoted as APTES-MGT.

## 2.4. Synthesis of EVA-g-OH compatibilizer

The grafted reaction was carried out in the molten state using a 50 ml internal mixer (Brabender® GmbH & Co. KG). The EVA, 0.1 wt% of DCP and 2 wt% of MAH were

introduced in the preheated mixer at 180°C and mechanically mixed at 30 rpm for 6 min, then a micro liter of water was dropped into the mixture in order to convert the anhydride function into diacide. After mixing, 2 wt% of 1,12 dodecanediol was added and mixed for 2 min. The product was taken from the mixer, solidified and ground into pellets.

## 2.5. Preparation of nanocomposites

The various formulations used in this study are summarized in Table 1. All nanocomposites were prepared by a two-step compounding process using a Brabender plastograph. First, a pre-dispersed MGT clay masterbatch was prepared at 180°C and 30 rpm. Then, the masterbatch was incorporated into the PVC/EVA matrix at a 50/50 proportion and mixed for 8 min. The final nanocomposites contain 3 wt% of MGT and 20 wt% of EVA-g-OH. After pelletizing, the nanocomposites granulates were compression molded using a hydraulic press at 190°C and 200 kg/cm<sup>2</sup> for 6 min.

**Table 1.** Sample designation

Designation	Formulation
E0	EVA
E1	PVC
E2	PVC/EVA
E3	PVC/EVA/Na <sup>+</sup> -MGT
E4	PVC/EVA/APTES-MGT
E5	PVC/EVA/EVA-g-OH
E6	PVC/EVA/EVA-g-OH/Na <sup>+</sup> -MGT
E7	PVC/EVA/EVA-g-OH/APTES-MGT

## 2.6. Fourier Transform Infrared spectroscopy (FTIR)

In this study, the chemical structures of the unmodified and modified MGT and EVA-g-OH were carried out using the infrared analysis on a PERKIN ELMER 1000 spectrophotometer controlled by a microcomputer. The spectra were recorded in the region of 4000 – 400 cm<sup>-1</sup> at resolution of 4 cm<sup>-1</sup> with 16 coadded scans.

## 2.7. Dynamic Rheological Analysis (DRA)

A Brabender plastograph (Brabender® GmbH & Co. KG) was used for the dynamic

rheological analysis. During mixing, it is possible to record changes in the torque and temperature with time. This torque is directly proportional to the viscosity of the molten matrix. Thus, monitoring the evolution with time and temperature makes it possible to follow the evolution of the viscosity and the state of the materials, as well as the chemical reactions taking place.

### **2.8. X-ray Diffraction (XRD)**

The X-ray diffraction was used to study the crystal structure of the clay as well as the changes of its interlayer distance. XRD analysis was performed at room temperature with copper radiation using a Phillips X'Pert diffractometer with a step size of  $0.02^\circ$  ( $2\theta$ ) and a rate of  $2.4^\circ$  ( $2\theta$ ) per minute. The X-ray beam was a  $\text{CuK}\alpha$  radiation ( $\lambda=1.54 \text{ \AA}$ ) using a 35 kV voltage generator and a 55 mA current.

### **2.9. Thermal analysis (TGA/DTA)**

Thermogravimetric analysis coupled with differential thermal analysis (TGA/DTA) measurements were performed on a TA instruments SDT Q600 under nitrogen atmosphere with a base purge flow of  $10 \text{ ml}\cdot\text{min}^{-1}$ , using sample weights of  $1.0 \pm 0.2 \text{ mg}$  in  $50 \mu\text{l}$  platinum crucibles, starting from  $25^\circ\text{C}$  and heating up to  $600^\circ\text{C}$ .

### **2.10. Mechanical properties**

Tensile properties were performed according to ASTM D 638 specifications. The testing was performed in a Zwick dynamometer at room temperature using a 0.5kN load cell at a testing speed of  $10 \text{ mm}\cdot\text{min}^{-1}$ . The micro-indentation measurements were carried out at room temperature using a Leitz Microhardness Tester equipped with a diamond square pyramid having an included angle at the tip of  $136^\circ$ . A load of 5 N was applied for 6 sec from the time of contact of the diamond until the load was removed.

### **2.11. Scanning Electronic Microscopy (SEM)**

SEM micrographs of the nanocomposites were observed on a JEOL JSM-6400 microscope with an acceleration voltage of 15kV and a magnification of 3000x. The nanocomposites were fractured in liquid nitrogen and the fracture surfaces were sputter coated with a thin layer of gold prior to examination.

### 3. RESULTS AND DISCUSSION

#### 3.1. FTIR analysis of ethylene vinyl acetate grafted an alcohol (EVA-g-OH)

The grafting of EVA was confirmed by FTIR spectroscopy. Figure 1 shows the FTIR spectra of EVA and EVA-g-OH. The characteristic band which appears at  $1736\text{ cm}^{-1}$  (Figure 1a) is attributed to the carbonyl groups of vinyl acetate. The spectrum of EVA-g-OH (Figure 1b) shows two additional bands at  $1752\text{ cm}^{-1}$  and  $1706\text{ cm}^{-1}$ , which are attributed to the carbonyl groups of the ester and the residual maleic acid, respectively [25]. These two bands do not appear in neat EVA spectrum.

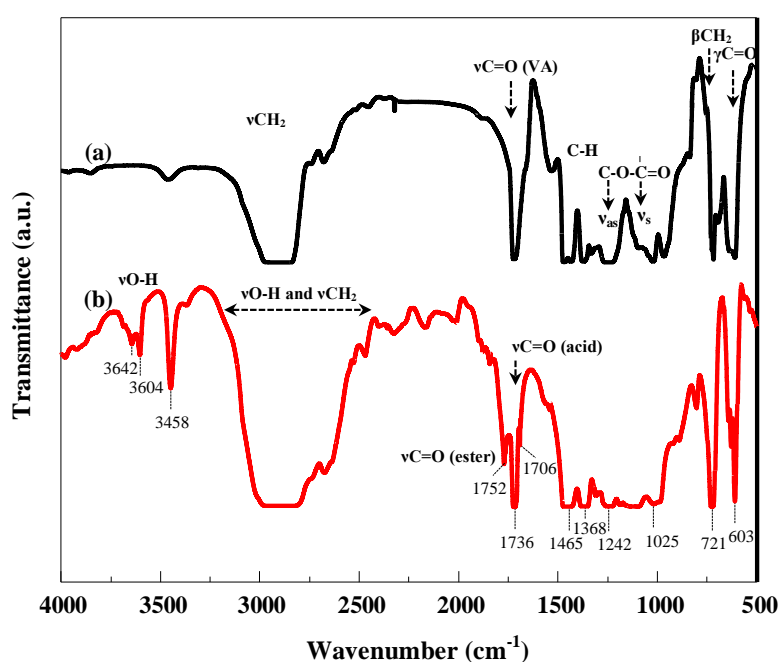


**Fig.1.** FTIR spectra of (a) neat EVA and (b) EVA-g-OH

#### 3.2. FTIR analysis of organomodified MGT

Figure 2 displays the FTIR spectra of  $\text{Na}^+$ -MGT,  $\text{ODTMA}^+$ -MGT and APTES-MGT. For  $\text{Na}^+$ -MGT (Figure 2a), the bands at  $3633$ ,  $3417$ ,  $1630$ ,  $1047$  and  $526\text{ cm}^{-1}$  are assigned to the presence of structural hydroxyl groups, the -OH stretching of water, the -OH deformation of water, Si-O stretching and Al-O-Si deformation, and also to deformation modes of O-H groups attached to various ions, e.g., aluminum and/or magnesium respectively [26]. The FTIR spectrums of  $\text{ODTMA}^+$ -MGT (Figure 2b) shows the presence of new absorption bands at  $3247$ ,  $2925$ ,  $2850$  and  $1472\text{ cm}^{-1}$  and are attributed to the symmetric and asymmetric stretching of  $\text{CH}_2$  or  $\text{CH}_3$ , and  $\text{CH}_2$  scissoring of alkylammonium, respectively [25]. The

position of the band related to the O-H bending vibrations of water molecules adsorbed on Na<sup>+</sup>-MGT shifted from 1630 cm<sup>-1</sup> to 1640 cm<sup>-1</sup> with ODTMA<sup>+</sup>-MGT. The shifting of the band reflects that the H<sub>2</sub>O content was reduced with the replacement of the hydrated cations by ODTMA<sup>+</sup> ions.

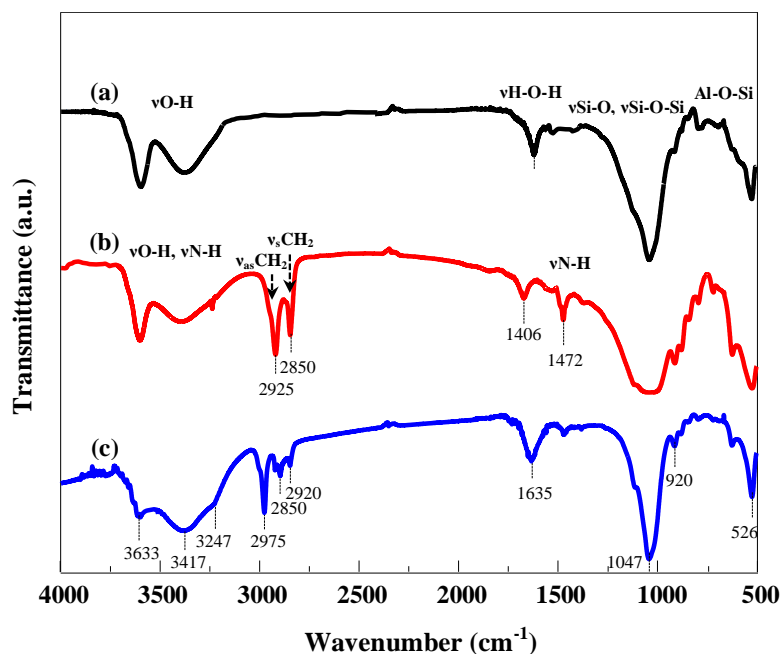


**Fig.2.** FTIR spectra of (a) Na<sup>+</sup>-MGT, (b) ODTMA<sup>+</sup>-MGT and (c) APTES-MGT

The efficiency of silanization was also investigated by FTIR spectroscopy. In Figure 2c, the band at 1640 cm<sup>-1</sup> found for ODTMA<sup>+</sup>-MGT shifted to 1635 cm<sup>-1</sup>. The band is ascribable to O-H groups of water molecules on the interlayer surface hydrogen bonded with silanol groups. The bands at 2975, 2920 and 2850 cm<sup>-1</sup> are due to aliphatic C-H stretching vibrations of residual alkylammonium and silane molecules. This confirms the effectiveness of intercalation/silanization of ODTMA<sup>+</sup>-MGT with APTES.

### 3.3. XRD analysis of MGT

The diffraction patterns of the different samples are shown in Figure 3. The peak at  $2\theta = 6.9^\circ$  observed for Na<sup>+</sup>-MGT (Figure 3a) corresponds to the periodicity in the direction perpendicular to the (001) plane of the clay [27]. The d-spacing value ( $d_{001}$ ) was calculated from the peak position of XRD pattern using Bragg's law [28]. The Na<sup>+</sup>-MGT sample has a spacing  $d_{001} = 12.79$  nm. According to the literature, montmorillonite has one or more layers of water adsorbed on the surface of the sheets, which causes an increase in the interlayer

distance of 3 Å knowing that the basal spacing of anhydrous silicate is 9.6 Å [29].

The presence of the alkylammonium and the silane molecules leads to an increase of the interlayer distance compared to the original Maghnite. The value of  $2\theta$  basal spacing was observed at  $2\theta = 3.2^\circ$  for both ODTMA<sup>+</sup>-MGT and APTES-MGT samples (Figure 3b and Figure 3c). The  $d_{001}$  increased from 12.79 to 28.78 Å. This implies that the Maghnite interlayer spacing has expanded due to the intercalation/grafting of alkylammonium surfactant and silane coupling agent.

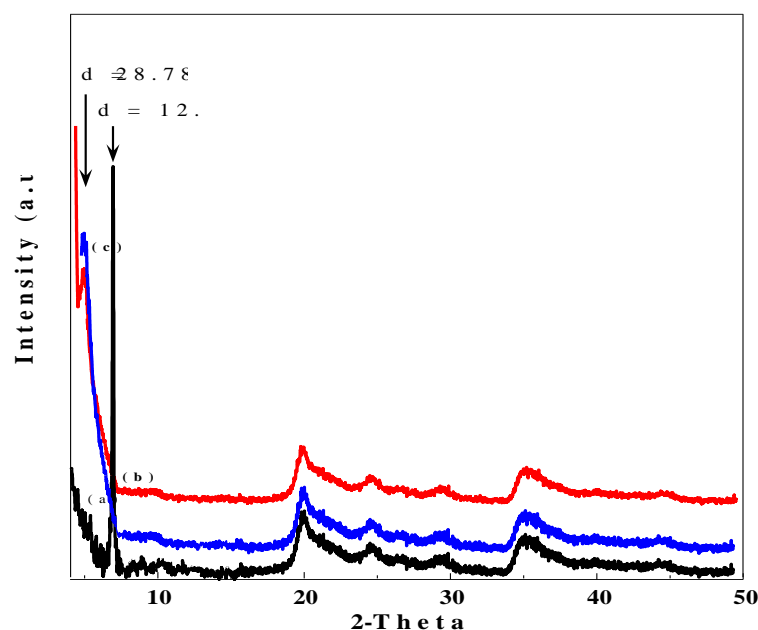


**Fig.3.** XRD patterns of (a) Na<sup>+</sup>-MGT, (b) ODTMA<sup>+</sup>-MGT and (c) APTES-MGT

### 3.4. Dynamic Rheological Analysis

Figure 4 shows the plastograms of PVC/EVA blend and nanocomposites at 180°C and 60 rpm/min. The fusion process of the PVC/EVA blend was completed at zone III and zone IV, respectively. The fusion process of the component, in this case, is initiated at zone III remind that viscosity is a direct function of torque which accounts for the torque increment. As result, the increase in viscosity coupled to shear, generates frictional heat accumulation [30]. This is due to the increase of the temperature of the melt. Thus, the point of the fusion is observed at zone V and the fusion continues.

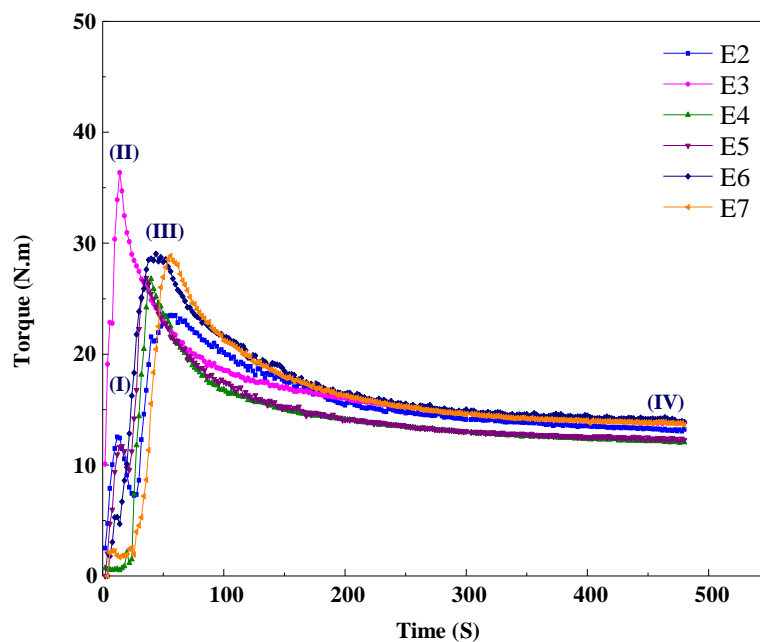


**Fig.4.** Brabender plastograms of PVC/EVA, PVC/EVA/Na<sup>+</sup>-MGT, PVC/EVA/APTES-MGT, PVC/EVA/EVA-g-OH, PVC/EVA/EVA-g-OH/Na<sup>+</sup>-MGT and PVC/EVA/EVA-g-OH/APTES-MGT

In Figure 4 the increase of the viscosity in the fusion torque obtained for PVC/EVA nanocomposites filled with treated MGT, compared to those of neat components, are explained by the increase of the friction in the system and the increase in the transfer of heat and shear through PVC and EVA. The time position of the maximum value of the PVC/EVA/Na<sup>+</sup>-MGT is higher than that of PVC/EVA/APTES-MGT. This may be due to the agglomeration of the filler particles. The addition of fillers to the blend causes an increase in the shear stresses and causes a substantial increase in the torque. Moreover, Figure 4 shows that there is an increase in the maximum values of the torque of compatibilized PVC/EVA nanocomposites compared with PVC/EVA uncompatibilized nanocomposites

### 3.5. X-Ray diffraction of nanocomposites

Figure 5 shows the XRD diffraction patterns of PVC/EVA blend and nanocomposites. For the PVC/EVA nanocomposites, Figure 5 shows a displacement of the peak to a lower angle  $2\theta = 19.2^\circ$  corresponding to  $d = 4.68$  nm. The disappearance and the enlarged basal spacing values clearly indicate that a macromolecular chain is intercalated into the galleries of the Maghnite, thus contributing to an exfoliation state. The disappearance of the corresponding

peak of the nanocomposites is due to the high degree of exfoliation of the nanofiller in the polymer matrix [1]. A matching between the polarity of PVC and nanoclay facilitates the diffusion of the polymeric chains into the layers of the nanoclay and leads to the exfoliation state [31,32]. However, the nanocomposites which contain the compatibilizer, show an exfoliated nanostructure due to penetration of the polymer chains into the MGT galleries. It is evident that in the WAXS patterns of the nanocomposites the presence of the compatibilizer reduces the intensity of the peak [18]. The experimental results of the XRD analysis of the PVC/EVA compatibilized and non compatibilized nanocomposites show no change in the position of the basal peaks, but the broader and the higher peaks become weaker or disappear.

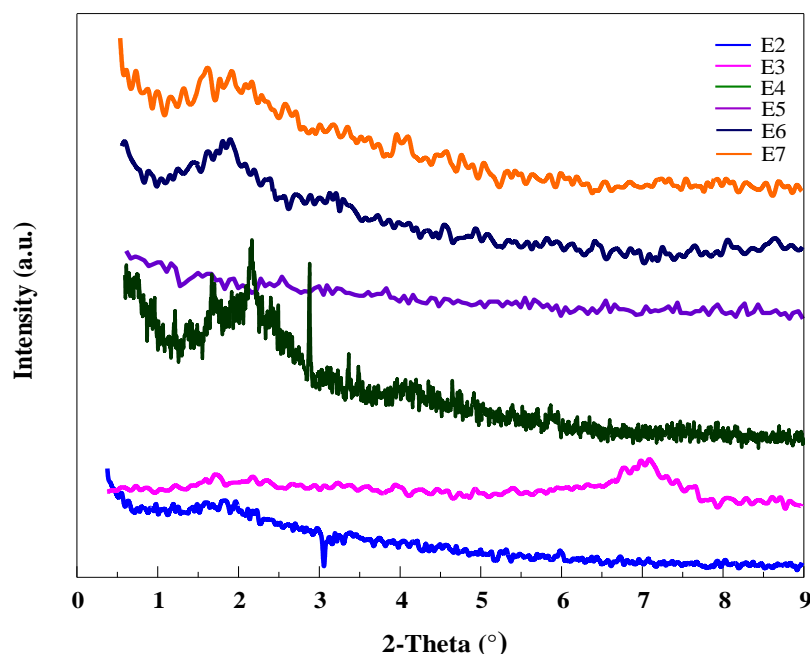


**Fig.5.** XRD patterns of PVC/EVA blend, PVC/EVA/ $\text{Na}^+$ -MGT, PVC/EVA/APTES-MGT, PVC/EVA/EVA-g-OH, PVC/EVA/EVA-g-OH/ $\text{Na}^+$ -MGT, PVC/EVA/EVA-g-OH/APTES-MGT nanocomposites

### 3.6. TGA/DTA analysis of the nanocomposites

Figure 6a and Figure 6b represent the TGA thermograms of the PVC and EVA neat polymers, respectively. The TGA thermogram of EVA (Figure 6a) shows two weight losses; the first degradation step, between 250 and 400°C corresponds to the elimination of a molecule of acetic acid (desacetylation), which leads to the creation of an ethylene structure on the rest of the carbon chain (formation of a polyunsaturated hydrocarbon chain). The second

degradation, step in the temperature range between 400 and 500°C, is due to the formation of “transvinyls”, accompanied by the scission of the principal chain and the formation of polyene. The “trans” configuration of vinyl double bonds favors an intermolecular transversal concatenation (cross-linking) of molecules [33]. The DTA curve (Figure 6a) shows a large endothermic signal during deacetylation and a large exothermic signal during the formation of an unsaturated backbone (polyene). The TGA thermogram of PVC (Figure 6b) recorded in this study is similar to the curve obtained by other authors [1,4,5,34]. The TGA weight loss profiles indicate that three steps decomposition processes are occurring. The first step, in the temperature range between 250 and 340°C, involves a dehydrochlorination reaction by the loss of HCl that was followed by the formation of conjugated double bonds, accompanied by the formation of low quantities of hydrocarbons [35]. The second step in the range of (400-470°C), is due to the condensation and fragmentation of polyene sequences. The third step (470 - 550°C) is due to the evolution of the degradation and the formation of substituted aromatic molecules [36]. The DTA curve (Figure 6b) shows three endothermic peaks during the dehydrochlorination, the formation of polyene sequences and aromatic substances.

The TGA curves of PVC/EVA blend are shown in Figure 6c. The recorded TGA plot shows three distinct degradation regions which suggest the coexistence of degradation of PVC and EVA simultaneously. The first step is between 250 and 440°C, the second step is between 440 and 500°C and the third step is between 500 and 570°C. This indicates that the thermal stability of PVC increases by mixing it with EVA. The DTA curve reveals one large exothermic effect and two small endothermic effects during the three decomposition steps. The TGA curve for EVA/PVC/EVA-g-OH blend sample is shown in Figure 6d. It is clear that, the recorded TGA plot shows three degradation regions. It is also clear that the degradation behavior of PVC is enhanced by the addition of EVA-g-OH in the blend. The DTA curve shows two endothermic signals during the first and the last steps of the decomposition, and one small exothermic signal during the second step of the decomposition of the blend.

The thermal behaviour of the uncompatibilized and compatibilized nanocomposites in the TGA test is presented in Figures 6e-6h. It is shown that by the addition of nanoparticles, the

---

onset of the temperature of the decomposition has been shifted to higher values. The recorded TGA plots for all nanocomposites samples show three degradation steps. The highest shift for the onset temperature of decomposition is attributed to the compatibilized nanocomposites containing the modified nanoclay (Figure 6h). The maximum onset temperatures recorded are 305, 460 and 520°C for the first, second and third degradation steps respectively. For all the other nanocomposites (Figures 6e-6g), we noticed also three degradation steps. The first degradation step is between 270 and 440°C, the second step is between 440 and 520°C and the last degradation step is above 510°C. Based on these results, it was concluded that the thermal stability of the nanocomposites was influenced by the modification of the clay and the addition of the compatibilizer. The crucial parameter for improvement of the thermal stability of these nanocomposites was assigned to the homogeneous dispersion of the nanoclay in the blend and a better interaction between the different constituents. The DTA curves reveal two small endothermic effects and one large exothermic effect during the three degradation steps of the nanocomposites.

It is shown that by addition of EVA and nanoparticles of MGT, the temperature of decomposition was shifted to higher values. This shift of the decomposition temperature is attributed to the sample containing EVA and MGT. It is known that thermal decomposition of quaternary ammonium salt, on the basis of Hofmann degradation mechanism, is accompanied by the formation of H<sup>+</sup> and traces of HCl, and that, during this process, the presence of H<sup>+</sup> and HCl catalyzes the polymer matrix degradation and accelerates the dehydrochlorination of the PVC chains [4,32]. Beyer [37] observed a strong color change which occurred in the presence of OMMT in PVC/EVA nanocomposites. This change of color was an effect of chain stripping of PVC by dehydrochlorination. The improvement of the thermal stability of PVC/EVA blends is linked to the molecular level miscibility of the polymeric components in the blend.

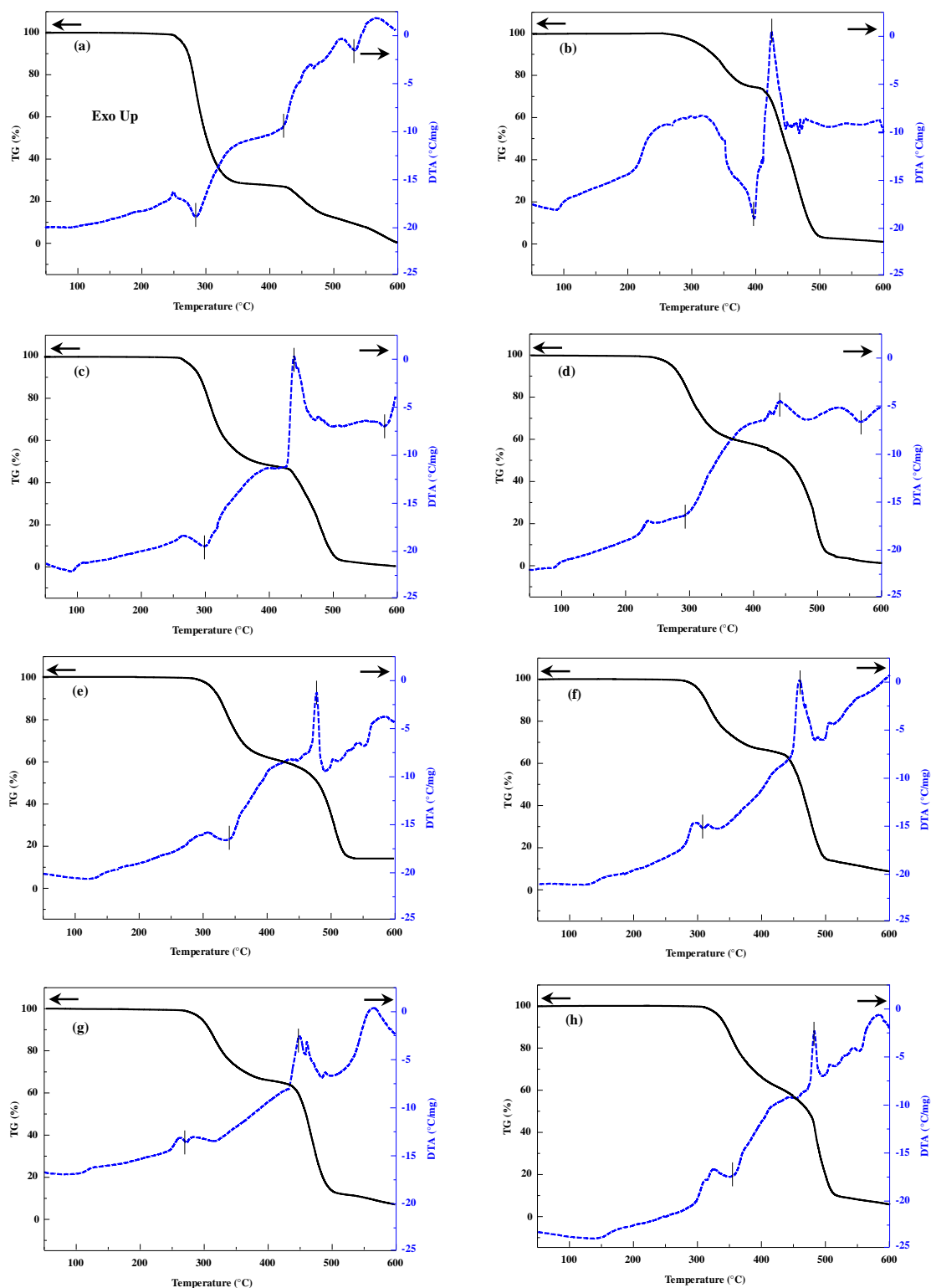


**Fig.6.** TGA and DTA curves of (a) PVC, (b) EVA, (c) PVC/EVA blend, (d) PVC/EVA/EVA-g-OH, (e) PVC/EVA/ $\text{Na}^+$ -MGT, (f) PVC/EVA/APTES-MGT, (g) PVC/EVA/EVA-g-OH/ $\text{Na}^+$ -MGT and (h) PVC/EVA/EVA-g-OH/APTES-MGT nanocomposites

### 3.7. Mechanical properties

Figure 7 shows that the incorporation of PVC into the EVA results in a higher tensile strength than that of neat EVA, and the addition of EVA to the PVC resulted in an improvement of the tensile strain.

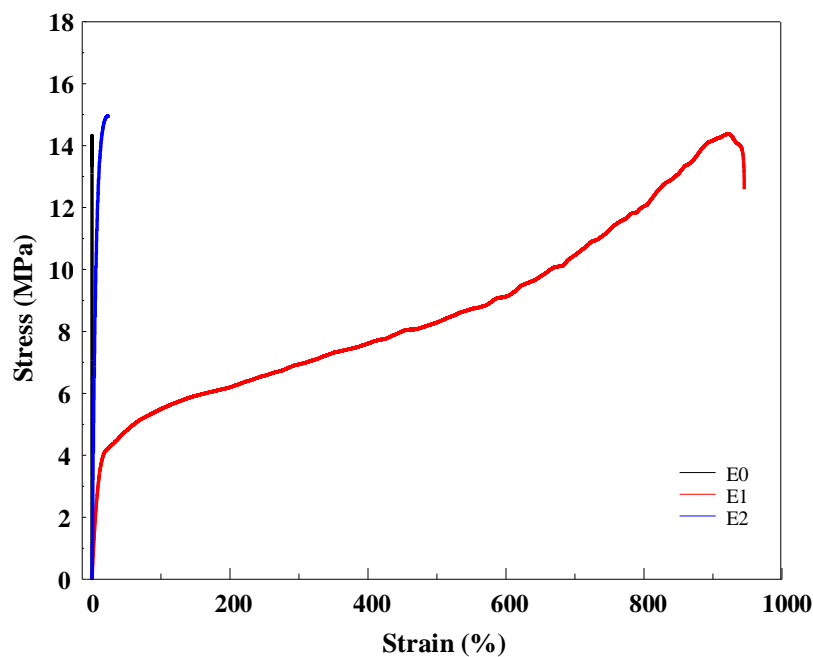


Fig.7. Stress-Strain curves of PVC, EVA and PVC/EVA blend

We can see from Figure 8 that both strength at break and modulus are slightly higher in nanocomposites than in the blend as consequence of the higher stiffness of the inorganic clay, and due to an exchange of interactions between the interfacial agents within material [1]. A moderate increase of the elastic modulus of the nanocomposites, can be attributed to the formation of filler platelets. The fracture appears to be not related to the nature of the clay but rather to its dispersion within the nanocomposite.

A significant increase in the stress at break and good strain properties which are observed are due to the good interaction between the hydroxyl functionalized ammonium cations used to modify the clay, and the acetate functions of EVA [38]. High values of Young's modulus found indicate a large extent of exfoliation.

From Figure 9 we can see that the addition of the compatibilizer influences the mechanical properties of the nanocomposites. This decrease of the tensile strength and increase of the elongation at break, are due to the functionality of the copolymer which promotes the

interaction between the polymeric phases and the clay, and creates a certain adhesion between the various phases, reducing hence the interfacial tension [1].

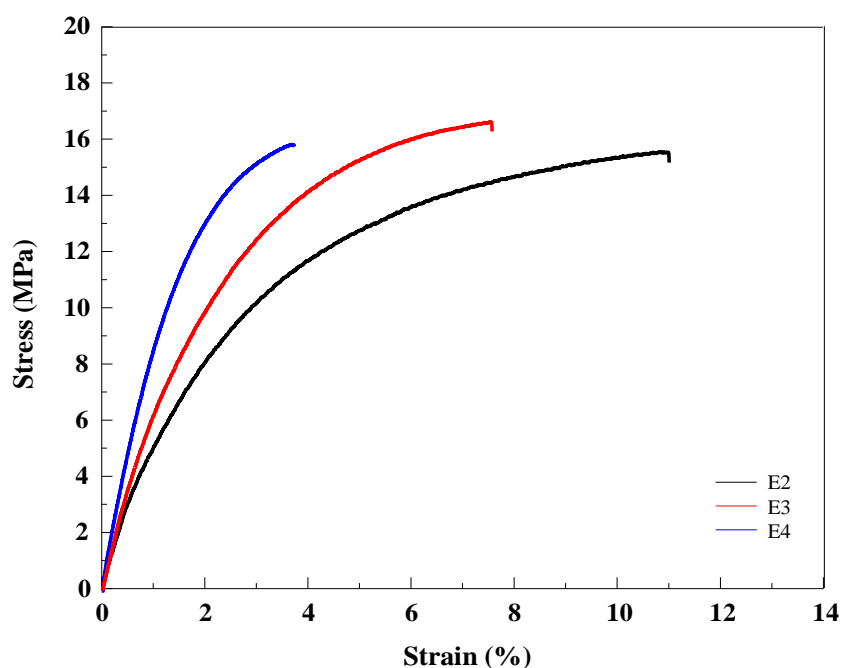


**Fig.8.** Stress-Strain curves of PVC/EVA blend, PVC/EVA/Na<sup>+</sup>-MGT and PVC/EVA/AMPTES-MGT nanocomposites

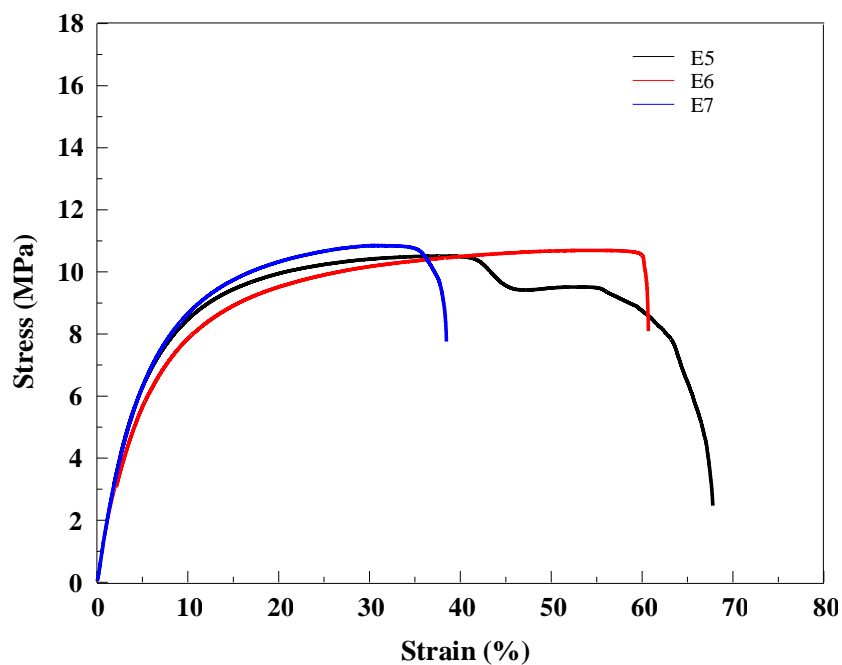


**Fig.9.** Stress-Strain curves of PVC/EVA/EVA-g-OH/Na<sup>+</sup>-MGT, PVC/EVA/EVA-g-OH/APTES-MGT nanocomposites

### 3.8. Microhardness of the nanocomposites

The measurement of the microhardness is a simple and important technique used to examine the morphology and microstructure of polymers. The experimental values of microhardness were determined using a Leitz microhardness tester.

The films were indented with a microindenter having a pyramidal shape with an angle of 136° and loaded by a force P. An indentation time of 6 s was used to minimize the creep of the sample under the indenter. The microhardness (H) is given by the following relationship [39]:

$$H = K.P/d^2$$

where:

K is a geometrical factor and is equal to 1.854 (according to [39]) d: is the diagonal of the indentation in meters.

Figures 10, 11 illustrate the correlation between microhardness, degree of crystallinity and Young's modulus of the investigated samples. In semi-crystalline polymers, the inclusion of a rubber phase, the crystal thickness, and the degree of crystallinity, influence the hardness value [40,41]. In our study, a remarkable increase in hardness was obtained with increasing the degree of crystallinity (Figure 10), this is in agreement with the results found by Azzurri et al [42].

The increase in hardness and crystallinity, shown in Figure 10, can be related to the crystalline nature of the compatibilizer (EVA-g-OH). It is clear from Figure 10 that, when the compatibilizer was added to this blend, an increase in the crystallinity and a simultaneous decrease in the hardness were obtained. On the other hand, the addition of the clay to the blend leads to a remarkable increase in the crystallinity and the hardness.

The correlation between microhardness and Young's modulus derived from tensile testing in this study is shown in Figure 11. The microhardness values of PVC/EVA blends indicate a tendency to increase with Young's modulus. In most cases, the hardness increase modulated by the chain extension of the lamellae, parallels the increase in stiffness. When measuring H, the plastic deformation of lamellae at larger strains, depends mainly on crystal thickness and perfection. But, in the case of the elastic modulus, the sizable role is played by the amorphous layer reinforced by tie molecules, which is deformed elastically at small strains.

For the blend structural properties, the effect of strain rate in addition to the compatibilizer effects, changes in the overall crystallinity, blend components interaction, etc... [43].

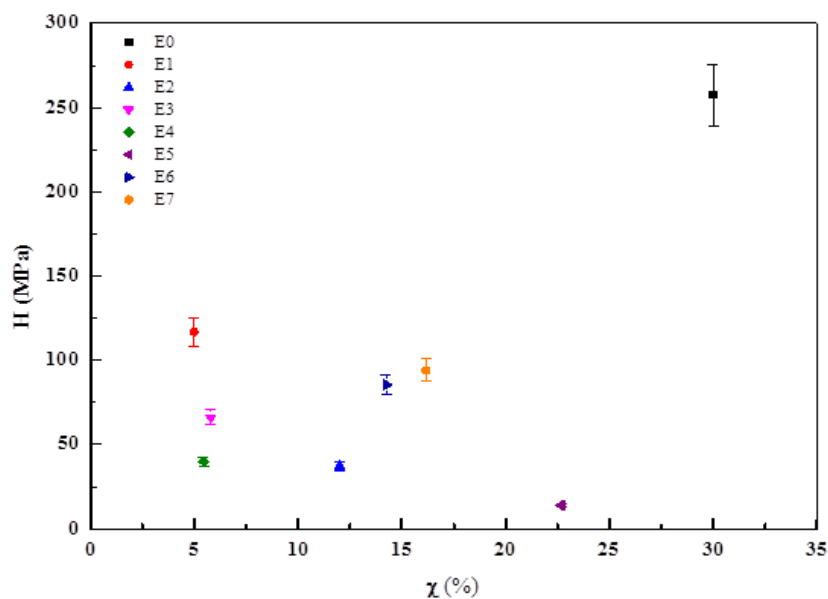


**Fig.10.** Variation of microhardness, H as a function of the degree of crystallinity of PVC, EVA, PVC/EVA, PVC/EVA/EVA-g-OH, PVC/EVA/Na<sup>+</sup>-MGT, PVC/EVA/APTES-MGT, PVC/EVA/EVA-g-OH/Na<sup>+</sup>-MGT and PVC/EVA/EVA-g-OH/APTES-MGT nanocomposites

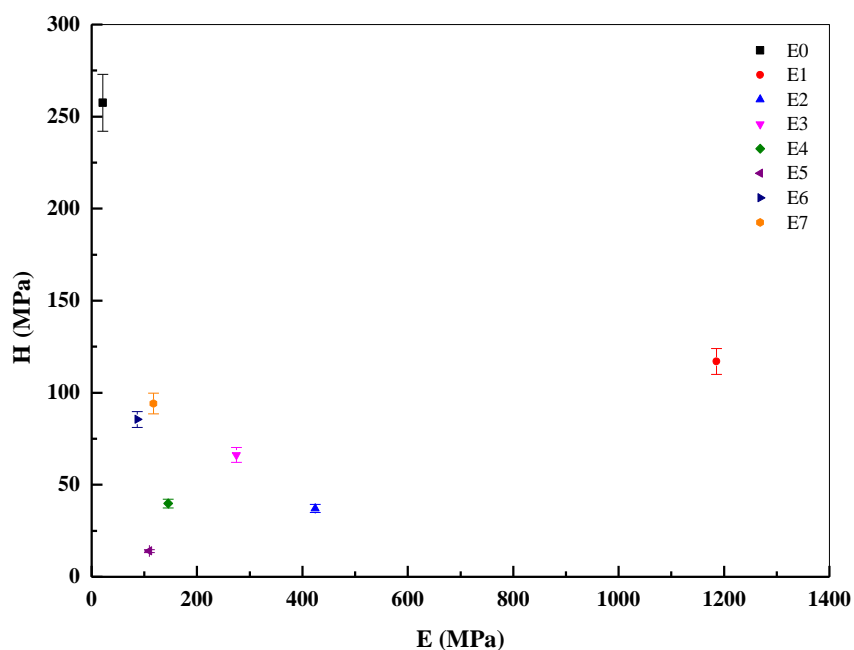


**Fig.11.** Variation of microhardness, H as a function of Young's modulus of PVC, EVA, PVC/EVA, PVC/EVA/EVA-g-OH, PVC/EVA/Na<sup>+</sup>-MGT, PVC/EVA/APTES-MGT, PVC/EVA/EVA-g-OH/Na<sup>+</sup>-MGT and PVC/EVA/EVA-g-OH/APTES-MGT nanocomposites

### 3.9. SEM Analysis of nanocomposites

Scanning electron microscopy was used to analyze the state of dispersion of the clay in the nanocomposites. Figure 12 shows the SEM micrographs of the fracture surfaces of PVC/EVA blend and those of the nanocomposites. The SEM micrograph of PVC/EVA (Figure 12a) shows a consistency and homogeneously distribution of the phases in the blend which resulted in a smoother fracture surface. We can see that an acceptable state of dispersion of the filler is scattered on the fracture surface. The presence of the pores on the fracture surface of the nanocomposites is due to the incompatibility between APTES-MGT and the polymer matrix (Figure 12b) [5].

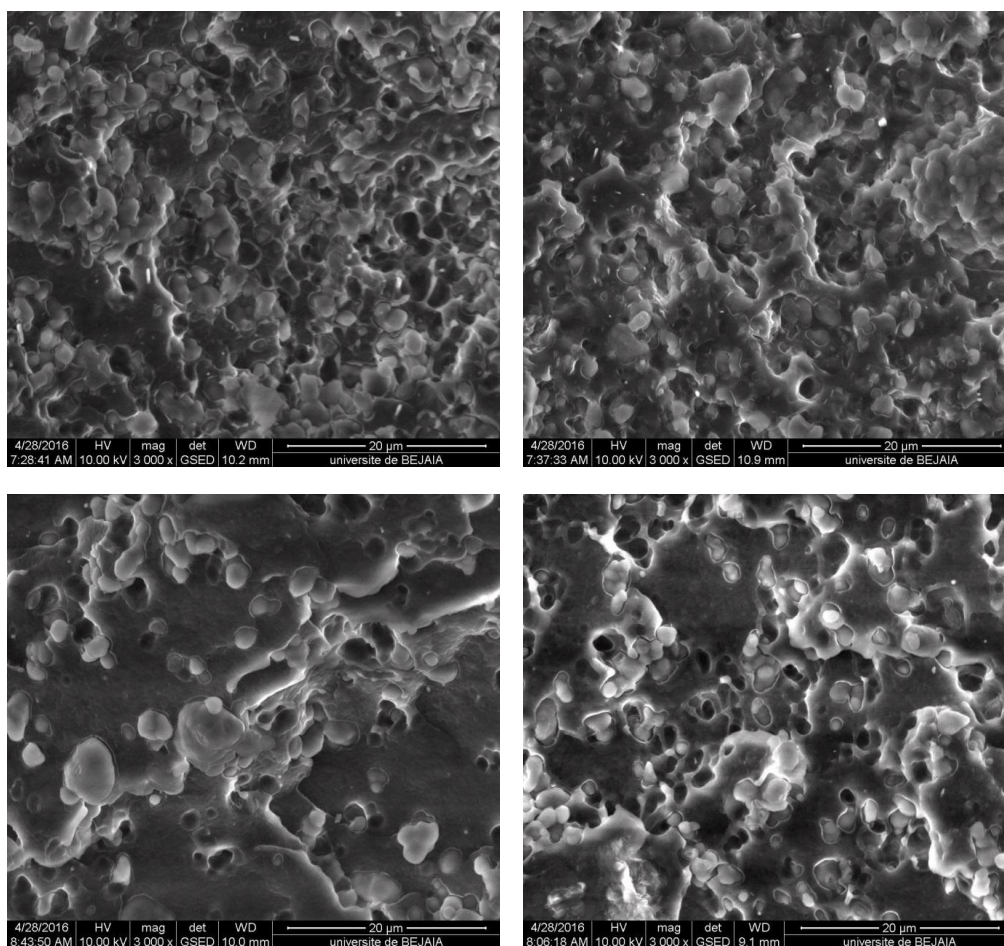


**Fig.12.** SEM micrographs of (a) PVC/EVA blend, (b) PVC/EVA/APTES-MGT, (c) PVC/EVA/EVA-g-OH and (d) PVC/EVA/EVA-g-OH/APTES-MGT nanocomposites

The SEM micrographs show that in the PVC/EVA compatibilized nanocomposite (Figure 12c-12d), the effect of the nature of the compatibilizer on the state of the dispersion,

is reflected. We observe white particles and some nodules dispersed within the matrix. The presence of the compatibilizer leads to the reduction of the size of the phases resulting from a good interfacial adhesion and improvement of the dispersion. On the other hand, it is observed the APTES-MGT is coated with a layer of the polymer which indicates an improved compatibility of the blend and a good dispersion of the clay [44].

#### 4. CONCLUSIONS

Nanocomposites based on Poly(vinyl chloride)/ethylene vinyl acetate copolymer (PVC/EVA) blend containing Maghnite nanoclay (MGT) were prepared by the melt-compounding method. The influence of MGT clay modification on the rheological, structural, mechanical and morphological properties was investigated. The compatibilization effects imparted by alcohol grafted ethylene vinyl acetate (EVA-g-OH) for PVC/EVA/MGT nanocomposites, were also studied.

- 1) It was observed, through thermogravimetric analysis (TGA/DTA), a considerable improvement in the thermal properties and a consequent increase in the thermal stability.
- 2) From XRD analysis the results showed that PVC and EVA chains were intercalated into the gallery of the nanoclay to form an exfoliated nanocomposites blend.
- 3) The X-ray diffraction analysis clearly showed that the introduction of the octadecyltrimethylammonium bromide and  $\gamma$ -aminopropyltriethoxysilane into the Na<sup>+</sup>-MGT gallery, allowed the basal spacing to increase, and this was proved by the X-ray diffraction results.
- 4) The incorporation of the modified MGT into the PVC/EVA blend leads to an increase of the thermal stability of the nanocomposites.
- 5) It was also found that the addition of the nanoclay to the blend enhanced the mechanical properties.
- 6) The SEM microphotographs showed that the MGT layers were homogeneously dispersed in the EVA matrix and in the interface between the PVC and EVA, which indicates that the MGT has a better compatibility with EVA.

## 5. ACKNOWLEDGEMENTS

The authors would like to thank « la Direction Générale de la Recherche – Algérie » for financial support.

## 6. REFERENCES

- [1] Ugel E, Giuliano G, Modesti M. poly (ethylene-co-vinyl acetate)/clay nanocomposites: Effect of clay nature and compatibilizing agents on morphological thermal and mechanical properties. *Soft Nanosci Lett.*, 2011, 1, 105–119.
- [2] John HH, Yu-Taek S, Ki HS, and Woo N. Morphology and dynamic mechanical properties of poly (acrylonitrile-butadiene styrene)/polycarbonate/clay nanocomposites prepared by melt mixing. *Compos Interfaces*, 2007, 14, 519–532.
- [3] Tcherbi-Narteh A, Hosur M, Jeelani S. Effects of different montmorillonite nanoclay loading on cure behavior and properties of diglycidyl ether of bisphenol an epoxy. *J Nanomater.*, 2016(2), 1-12.
- [4] Pagacz J, Pielichowski K. Preparation and characterization of PVC/montmorillonite nanocomposites-a review. *J Vinyl Addit Techn.*, 2009, 15 (2), 61-76.
- [5] Chuayjuljit S, Thongraar R, Saravari O. Nanocomposites preparation and properties of PVC/EVA/ organomodified montmorillonite. *J Reinf Plast Compos.*, 2008, 27, 431.
- [6] Leszczynska A, Pielichowski K. Application of thermal analysis methods for characterization of polymer/montmorillonite nanocomposites. *J Therm Anal Cal.*, 2008, 93(3), 677–687.
- [7] Kristóf B, Péter M, Béla P. Thermoplastic starch/layered silicate composites: Structure, interaction, properties. *Compos Interfaces*, 2006, 13, 1–17.
- [8] Christopher ML, Graham CL, Roger NR, and Arthur NW. Evaluation of an alternative modification route for layered silicates and synthesis of poly(styrene) layered silicate nanocomposites by in-situ suspension polymerization. *Compos Interfaces*, 2007, 14, 361–386.
- [9] Resende D, Dornelas C, Tavares MIB, and Lucio C. Preparation of modified montmorillonite with benzethonium and benzalkonium chloride for nanocomposites preparation. *Chem Chem Technol.*, 2009, 3, 4.

- 
- [10] Wang T, Liu D, Xiong C. Synthesis of EVA-g-MAH and its compatibilization effect to PA11/PVC blends. *J Mater Sci.*, 2007, 42, 3398–3407.
- [11] Imren D, Boztug A, Yılmaz E, Zengin HB. Viscometric investigation of compatibilization of the poly(vinyl chloride)/poly(ethylene-co-vinyl acetate) blends by terpolymer of maleic anhydride–styrene–vinyl acetate. *J Mol Struct.*, 2008, 891, 329–332.
- [12] Boussoum MO, Bensemra NB. Reduction of the additives migration from poly vinyl chloride films by the use of permanent plasticizers. *J Geosci Environ Protect.*, 2014, 2, 49–56.
- [13] Hernandez R, Pena JJ, Irusta L, and Santamaria A. The effect of a miscible and an immiscible polymeric modifier on the mechanical and rheological properties of PVC. *Eur Polym J.*, 2000, 36, 1011–1025.
- [14] Liu Y, Xie BH, Yang W, and Zhang W. Morphology and fracture behaviour of poly (vinyl chloride)/ ethylene-vinyl acetate copolymer blends. *Polym Test.*, 2007, 26, 388–395.
- [15] Coleman MM, Moskala EJ, Painter PC, et al. A Fourier transform infra-red study of the phase behaviour of polymer blends. Ethylene-vinyl acetate copolymer blends with poly (vinyl chloride) and chlorinated polyethylene. *Polymer*, 1983, 24, 1410–1414.
- [16] Michalski MC, Hardy JL, Saramago BJV. On the surface free energy of PVC/EVA polymer blends: Comparison of different calculation methods. *J Colloid Interface Sci.*, 1998, 208, 319–328.
- [17] Soudais Y, Moga L, Blazek J, and Lemort F. Coupled DTA–TGA–FT-IR investigation of pyrolytic decomposition of EVA, PVC and cellulose. *J Anal Appl Pyrolysis*, 2007, 78, 46–57.
- [18] Goodarzi V, Jafari SH, Khonakdar HA, and Ghalei B. Assessment of role of morphology in gas permselectivity of membranes based on polypropylene/ethylene vinyl acetate/clay nanocomposite. *J Membr Sci.*, 2013, 445, 76–87.
- [19] An Q F, Qian JW, Sun HB, and Wang LN. Compatibility of PVC/EVA blends and the pervaporation of their blend membranes for benzene/cyclohexane mixtures. *J Membr Sci.*, 2003, 222, 113–122.
- [20] Bureau E, Cabot C, Marais S, and Saiter JM. Study of the  $\alpha$ -relaxation of PVC, and 50/50 EVA70/PVC blend. *Eur Polym J.*, 2005, 41, 1152–1158.

- 
- [21] Thaumaturgo C, Monteiro EC. Thermal stability and miscibility in PVC/EVA blends. *J Therm Anal.*, 1997, 49, 247-254.
- [22] Corradini E, Rubira FA, Muniz EC. Miscibility of PVC/EVA hydrolyzed blends by viscosimetric, microscopic and thermal analysis. *Eur Polym.*, 1997; 33, 1651–1658.
- [23] Ren J, Huang Y, Liu Y, and Tang X. Preparation, characterization and properties of poly (vinyl chloride)/compatibilizer/organophilic–montmorillonite nanocomposites by melt intercalation. *Polym Test.*, 2005, 24 (3), 316–323.
- [24] Rzayev MO. graft copolymers of maleic anhydride and its isostructural analogues: high performance engineering materials. *Int Rev Chem Eng.*, 2011, 3, 153–215.
- [25] Bellamy LJ. *The infrared spectra of complexes molecules*, John Wiley & Sons. New York, 1984.
- [26] Frost RL, Mendelovici E. Modification of Fibrous Silicates Surfaces with Organic Derivatives: An Infrared Spectroscopic Study. *J Colloid Interface Sci.*, 2006, 294 (1), 47–52.
- [27] Yoshiaki F. X-Ray Diffraction study of aqueous montmorillonite emulsions. *Clays Clay Miner.*, 198, 32(4), 320–326.
- [28] David IF, Shankland K, McCusker LB. *Structure determination from powder diffraction data*. Oxford university press, Oxford, 2002.
- [29] Yamada H, Nakazawa H, Yoshioka K, and Fujita T. Smectites in the montmorillonite-beidellite series. *Clay Miner.*, 1991, 26, 359–369.
- [30] Mousa A. Studies on rheological behaviour of thermoplastic elastomer derived from PVC and NBR using Torque rheometry. *Iran Polym J.*, 2004, 13 (6), 455-461.
- [31] Peprnicek T, Duchet J, Kovarova L, and Malac J. Poly (vinyl chloride)/clay nanocomposites: X-ray diffraction, thermal and rheological behavior. *Polym degrad stab.*, 2006, 91, 1855–1860.
- [32] Saeedi M, Ghasemi I, Karrabi M. Thermal degradation of poly (vinyl chloride): Effect of nanoclay and low density polyethylene content. *Iran Polym J.*, 2011, 20, 423–432.
- [33] Munteanu D, Turcu SJ. Evaluation of kinetic parameters of the thermal decomposition of polyethylene-vinyl acetate graft copolymers, *Thermal Anal.*, 1981, 20, 281.
- [34] Alexandre M, Dubois P. Polymer-layered silicate nanocomposites: preparation,

properties and uses of a new class of materials. *Mater Sci Eng.*, 2000, 28, 1–63.

[35] Miranda R., Yang J, Roy CH, and Vasile C. Vacuum pyrolysis of PVC - I. Kinetic study. *Polym degrad stab.*, 1999, 64, 127–144.

[36] Marcilla A, Beltrán M. Thermogravimetric kinetic study of poly(vinylchloride) pyrolysis. *Polym degrad stab*, 1995, 117–124.

[37] Beyer G. Flame retardancy of thermoplastic polyurethane and polyvinyl chloride by organoclay. *J Fire Sci.*, 2007, 25, 65-78.

[38] Peeterbroeck S, Alexandre M, Jerome R, and Dubois Ph. Poly(ethylene-co-vinyl acetate)/clay nanocomposites: Effect of clay nature and organic modifiers on morphology, mechanical and thermal properties. *Polym Degrad Stab.*, 2005, 90, 288–294.

[39] Balta Calleja F J, Fakirov S. *Microhardness of Polymers; Solid State Science Series.* Cambridge. University Press: Cambridge, England.2000, 1, 3.

[40] Adhikari R, Michler GH, Cagliao ME, and Balta Calleja FJ .Micromechanical studies of styrene/butadiene block copolymer blends. *J Polym Eng.*, 2003, 23, 0250–8079.

[41] Santa Cruz C, Balta Calleja FJ. Mechanical properties and structure of glassy and semicrystalline random copolymers of poly (ethylene terephthalate) and poly (ethylene naphthalene-2,6-dicarboxylate). *J Mater Sci.*, 1992, 27, 2161–2164.

[42] Azzurri F, Flores A, Alfonso GC, and Balta Calleja FJ. Polymorphism of isotactic poly (1-butene) as revealed by microindentation hardness.1.kinetics of the transformation. *Macromolecules*, 2002, 35, 9069–9073.

[43] Balta Calleja FJ. *Characterization of Polymers in the Solid State Part B: Mechanical Methods.* Verlag Berlin Heidelberg: Springer, 1985, pp. 117-148.

[44] Hajir Bahrami S, Mirzaie Z. Polypropylene/Modified Nanoclay Composite-Processing and Dyeability Properties. *World Appl. Sci J.*, 2011, 13, 493–501.

**How to cite this article:**

Bouaziz I, Doufnoune R, Haddaoui N, Benachour D, Baltä-Calleja FJ. Effects of maghnite nanoclay modification and compatibilization on the physical and morphological properties of poly(vinyl chloride)/poly(ethylene-co-vinyl acetate) blends. *J. Fundam. Appl. Sci.*, 2019, 11(1), 315-349.